Finite Element Approach for the Design of Control Algorithms for Vertical Fin Buffeting Using Strain Actuation

Fred Nitzsche*
Carleton University
Department of Mechanical and Aerospace Engineering
1125 Colonel By Drive
Ottawa, Ontario, Canada, K1S 5B6

David G. Zimcik‡ and Sauro Liberatore†
National Research Council Canada
Institute for Aerospace Research
Ottawa, Ontario, Canada, K1A 0R6

Abstract

It is difficult to predict buffet loads during the design stage of an aircraft. The present work describes the control design method used to address this problem for the F/A-18 aircraft which is often subjected to high-intensity buffet loads that produce high accelerations at the tip the vertical fin during maneuvers at high angles of attack. A NASTRAN finite-element model was constructed to represent the dynamics of the structure at the low frequencies of interest. The aeroelastic frequency response analysis and the thermal analogy available in NASTRAN were used together in a two-step procedure to simulate the strain actuation. This analysis was conducted for each group of actuators to obtain the transfer functions between the two control inputs (actuation groups), the disturbance (buffet load), and the two output variables (a choice among four accelerometers and five strain-gauge positions). Three independent white noise signals limited by the frequency band between 0 and 120 Hz were used in development of a 2×2 MIMO system. The result was a control system using strain actuation to attenuate the dynamic response caused by buffet loads. The predicted results were compared to full-scale test results in the IFOST Program test facility in Australia. The results demonstrated significant reductions in the root-mean-square (RMS) values of the fin dynamic response measured by the strain transducer at the critical point for fatigue at the root were achieved under the most severe buffet condition.

Nomenclature

$A,\ldots,F,\Gamma$	state-vector system matrices (Equation 1)
G	open-loop transfer function matrix
G_c	closed-loop transfer function matrix
G_u	controller transfer function matrix
H	feedback transfer function matrix
K	full-state feedback gain matrix
L	Kalman filter estimator gain matrix
u	vector of control variables
v	transducer noise
w	buffet disturbance
$x, \hat{x}$	state vector, estimated state vector
y, y_v	feedback vector, idem noise contaminated
z, z_c	vector of performance metrics

Introduction

It is difficult to predict buffet loads during the design stage of an aircraft. One such example is the F/A-18 known in Canada as the CF-118. This twin-tail aircraft is often subjected to high-intensity buffet loads that produce accelerations in excess of 450 g at the tip the vertical fin during maneuvers at high angles of attack. An initial approach to minimize the problem included the introduction of a leading edge extension (LEX) fence. This fence has been added to the aircraft wing root to reduce buffeting by generating additional vortices that interact with the vertical tail and assure airflow attachment to the surface. However, at very high angles of attack, the vortices generated by the LEX fence break down before reaching the tail, generating an even more turbulent wake. The loads produced substantially contribute to the fatigue of the

* Associate Professor
‡ Head, Aeroacoustics and Structural Dynamics Group
† Research Engineer, presently at University of California at Los Angeles

Paper presented at the RTO AVT Symposium on "Active Control Technology for Enhanced Performance Operational Capabilities of Military Aircraft, Land Vehicles and Sea Vehicles", held in Braunschweig, Germany, 8-11 May 2000, and published in RTO MP-051.

tail structure, increasing the maintenance costs of the fighter.

This problem is of particular concern for those countries within The Technical Co-operation Program, (TTCP) that include the F/A-18 in their fleets. The TTCP is a program of technical collaboration and data exchange among five nations: Canada, the United States, Australia, United Kingdom and New Zealand. Of these participants, three countries, namely Canada, the United States, and Australia have initiated a collaborative research program aimed at solutions to the problem. The overall approach of the program is to develop an active control system that includes strain actuation using piezoelectric elements. However, the ability of the piezoelectric actuators to achieve control authority under the large aerodynamic buffet loads in a full-scaled aircraft needs to be demonstrated. Ground vibration tests were planned under the TTCP program with the objective of evaluating the performance of the "smart structures" solution. In this program, Australia contributed the test rig; Canada offered the input data information in the form of representative buffet time sequences measured in flight, and the United States provided the control system hardware. All TTCP partners contributed to the software design with unique control strategies.

The present work reports the control design strategy and the results obtained by the Canadian team in the closed-loop tests. The main objective was to investigate the most promising combination of sensors to achieve the required performance using the hardware installed on the airframe. This hardware was configured to accept a MIMO feedback control system with two inputs (consisting of a choice among several strain gauges and accelerometers distributed over the surface of the vertical fin to measure the performance of the system), and two outputs that drive two groups of piezoelectric actuators attached to both sides of the structure skin. Theoretical analyses with a NASTRAN model are presented in this paper to establish the control strategy. These analytical predictions re compared to full-scale tests carried out in the International Follow-on Structural Test (IFOST) rig in Melbourne, Australia. These tests represented an important milestone on the development of adaptive structures systems with application to aeroelastic problems because they were the first tests performed on a full-scale airframe to achieve aerodynamic buffet alleviation.

The objectives of the ground vibration test were: (1) to demonstrate active buffet suppression in a full-scale aircraft; (2) to measure vibration level reductions at different points on the tail, most significantly, at the critical points situated at the fin root where fatigue cracks have been spotted due to high bending stress; (3) to demonstrate piezoelectric control authority at full buffet loads; and (4) to measure vibration reduction at different flight conditions demonstrating the controller robustness under different excitation loads.

NASTRAN Model

Previous investigations were able to demonstrate that the first and the second natural modes of the structure contribute most significantly to the buffeting phenomenon.[1-4] Therefore, a NASTRAN finite-element model was built to represent as close as possible the dynamics of the structure at the low frequencies of interest. The finite element model of the vertical fin consisted of 1197 shell, 320 rod, 124 bar and 48 beam elements. In addition, 96 lumped mass elements located at selected grid points simulated the mass distribution. Also defined in the model were 8 scalar spring elements simulating both the structure boundary conditions and the stiffness of the rudder actuation system. The fin was restrained from moving in all degrees of freedom except for rotation with respect to the chordwise axis, where the springs emulated the stiffness of the bolts employed in fastening the fin to the fuselage. The shell elements were used to model both the skin and the internal stiffeners of the fin. The principal purpose of the rod elements was to simulate the piezoelectric patches working in unison in a push-pull configuration (out-of-phase extension-compression mode across the structure to generate bending). The latter elements were distributed along seven spanwise rows lying on the two skins of the fin, approximating the distribution of actuators suggested by the hardware designers to achieve authority over the first and second natural modes of the structure. The beam and bar elements had multiple functions, namely: (1) to connect the parts where the rod elements were interrupted to separate the actuators into two independent groups, (2) to perform a specific local structural reinforcement, and (3) to define the rudder structure. In the latter, only the rudder hinge was simulated because one is only interested in the rotational motion of the rudder. With this purpose, constraint cards were employed to average the displacement of the grids that represent the rudder hinge. Since the fin was a composite structure, several isotropic material properties were defined in the model.

Natural Frequencies and Mode Shapes

The NASTRAN Modified Givens Method was selected for searching the eigenvalues and eigenvectors associated with the free vibration of the structure. No structural or viscous damping was included as the motion-dependent aerodynamic loads were expected to

contribute most of damping observed by the system. The results of this analysis are shown in Table 1 for the natural modes of interest. The measured natural frequencies of the tested aircraft without the piezoelectric elements attached to its fin are also shown in the same table. When the mass of the piezoelectric elements was added to the model, the modal characteristics of the structure were slightly changed, and displayed in parentheses in Table 1.

Table 1: Natural Modes and Frequencies

mode shape description	model frequency (Hz)	actual frequency (Hz)
1st bending	15.8 (14.8)	15.7
1st torsion	42.6 (43.4)	43.3
rudder	47.6 (49.5)	49.6

In Figures 1 and 2, the mode shapes associated with the first two natural frequencies are plotted.

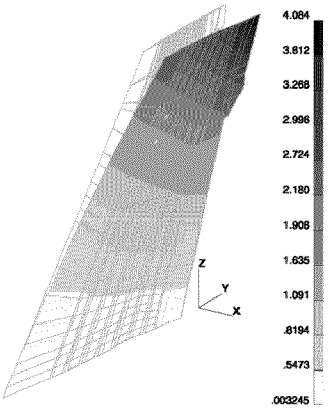

Figure 1: First Mode Shape (NASTRAN)

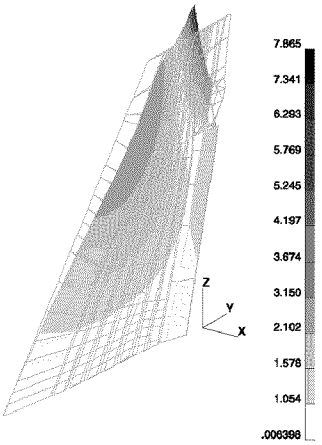

Figure 2: Second Mode Shape (NASTRAN)

Aeroelastic Model

According to the double lattice method,[5] steady horseshoe vortices and oscillatory doublets lying along bound vortex lines were used to model the lifting surfaces in subsonic flow. The vortices represent the steady flow effects, and the doublets represent the incremental effects due to the oscillatory motion. The lifting surface was divided into trapezoidal elements (boxes) arranged in strips parallel to the free stream. In the present model, two panels in the lower and upper parts of the vertical fin were defined. The lower panel was divided into 294 boxes: 21 in the chordwise and 14 in the spanwise direction including the rudder (84 boxes). The upper panel was divided into 168 boxes: 21 in the chordwise and 8 in the spanwise direction. The boxes were concentrated near the leading and trailing edges of the fin, and along the rudder hinge line. Using this refinement, the aspect ratio of the boxes was maintained at approximately one. To account for the forces arising from the body motion, slender body elements were provided in NASTRAN. Interference elements simulated the aerodynamic interference effects among the bodies and the lifting surfaces. In this model, nine slender bodies were used to represent the fuselage and the nacelle, and one interference element was defined to simulate the interference effects between the fuselage, nacelle and the vertical fin.

Strain Actuation

In order to simulate the strain actuation, the thermal analogy and the aeroelastic frequency response analysis available in NASTRAN were used together in a two-step procedure. First, a static and constant temperature field was applied only on the rod elements that represent the piezoelectric actuators. The temperature field had the same magnitude but opposite signs for elements lying on the opposite sides of the fin (no biasing considered). The reaction forces at the nodes of the rod elements that represent the piezoelectric actuators were obtained. The relative magnitude of these forces was used in a second step, where a forced frequency response analysis is performed. The forces obtained were applied in unison at the corresponding nodal points in order to simulate the external forces generated by the control system. This analysis was conducted for each group of actuators independently.

Open-loop Transfer Functions

Some earlier studies incorporating active control techniques to suppress aerodynamic buffeting focused on the classical aeroservoelastic approach, where the rudder was the actuation device.[6] However, adaptive structures provide an attractive solution to the

problem.[7-8] In principle, they allow for the development of sensor and actuator arrangements that are able to approximately perform independent modal state control, greatly improving the realization of a more efficient and robust closed-loop aeroelastic system.

The objective of the present work was to develop a control system using strain actuation to attenuate the dynamic response caused by buffet loads. Figure 3 shows the schematics of the closed-loop, output feedback control system analyzed. The buffeting pressure acting on the fin was treated as a disturbance of stochastic nature. The other input vector was due to the action of the two actuator groups which were patched to the structure to reproduce as closely as possible the strain distribution associated with each one of the first two modes referred in Table 1. Hence, each group had more control authority over one specific mode of the structure. Two vectors defined the system output: the first collected the signal produced by the sensor monitored for performance (normally the strain gauge located at the critical point for fatigue at the fin root), and the second the signal originated from the two sensors used for the feedback control.

The state-space representation of the referred system in the time domain is:

$$\begin{aligned} \dot{x} &= Ax + Bu + \Gamma w \\ y_v &= y + v = Cx + Du + v \\ z &= Ex + Fu \end{aligned} \tag{1}$$

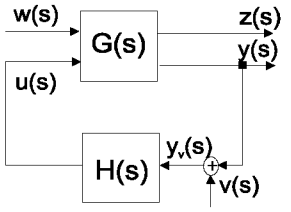

Figure 3: Output Feedback Active Control System (Disturbance Rejection).

In the present section, NASTRAN was employed to obtain the open loop transfer functions between the two control inputs (actuation groups G1 and G2), the disturbance (buffet load), and the two output variables (a choice among four accelerometers and five strain-gauge positions). For this, three independent white noise signals limited by the frequency band between 0 and 120 Hz were sent throughout the system between the chosen pair of input and output variables. The result was a 3×2 MIMO system where the third input variable was the disturbance load (Equation 2). In the present analysis, in order to reproduce the experimental setup better, the latter input was applied at a single point of the structure – the shaker position defined in the ground vibration tests.

$$\begin{Bmatrix} y_v(s) \\ z(s) \end{Bmatrix} = \begin{bmatrix} G_{11}(s) & G_{12}(s) \\ G_{21}(s) & G_{22}(s) \end{bmatrix} \begin{Bmatrix} u(s) \\ w(s) \end{Bmatrix} \tag{2}$$

The elements of the open-loop transfer function matrix were related to the original representation of the system shown in Equation 1 by:

$$\begin{aligned} G_{11}(s) &= C(sI - A)^{-1} B + D \\ G_{12}(s) &= C(sI - A)^{-1} \Gamma \\ G_{21}(s) &= E(sI - A)^{-1} B + F \\ G_{22}(s) &= E(sI - A)^{-1} \Gamma \end{aligned} \tag{3}$$

In order to calibrate the thermal loads used in the NASTRAN model to the actual piezoelectric loads, the magnitude of the white noise signal input to each actuation group was adjusted to reproduce the maximum values of strain obtained in the open-loop tests when each actuation group was operating alone and at full gain (saturation voltage).

System Identification using Numerical Data

Using the method explained in the previous section, the transfer functions listed in Equation 3 were numerically obtained. Polynomial fitting of the complex data was used to achieve an approximation for the transfer functions in the frequency interval of interest. Due to the fact that the state-space representation of a system was not unique, and those independent processes were used to obtain the individual transfer functions, the latter did not carry in general a common denominator. In order to proceed with the MIMO analysis, an optimization technique was employed to find the "best" fit in the least square sense of all transfer function elements bearing a common denominator.

In the present work, the buffet conditions presented in Table 2 were analyzed. Since flight conditions FC1 and FC3 were associated with the same flight speed and Mach number, the aeroelastic modes under the linear system assumption were identical, as were the related transfer functions. As representative examples of this analysis, the transfer functions between the strain gauge SG3 located at the critical point at the root and the three input signals (actuation groups G1 and G2, and the buffeting load) are depicted for FC1 in Figure 4.

Table 2: Buffet Conditions Analyzed

flight condition number	angle of attack (degrees)	dynamic pressure (psf)
FC1	12-16	225-300
FC3	20-24	225-300
FC5	28-32	300-350

Note: Sea-level conditions, Mach number 0.3.

Control Synthesis

The block diagram shown in Figure 5 provides a complete description of the active control system proposed in the present work. The regulator consists of a Kalman filter in-series with a Linear Quadratic Regulator (full-state feedback on estimated state values). A band-pass filter (not shown in the diagram) may be appended in-series to the controller output in some designs to cut either a DC signal (when strain is used for feedback) or an undesirable high-frequency response (to guarantee stability).

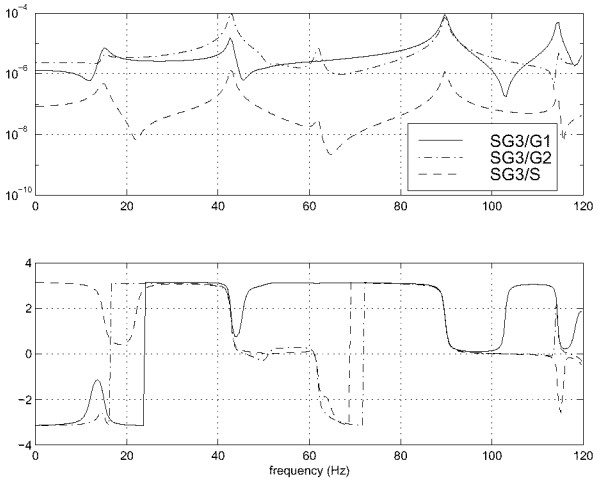

Figure 4: Complex Transfer Function between the Strain Gauge SG3 and Actuator Groups G1 & G2 and Shaker S. Upper Figure: Magnitude (1/lbf). Lower Figure: Phase (rad).

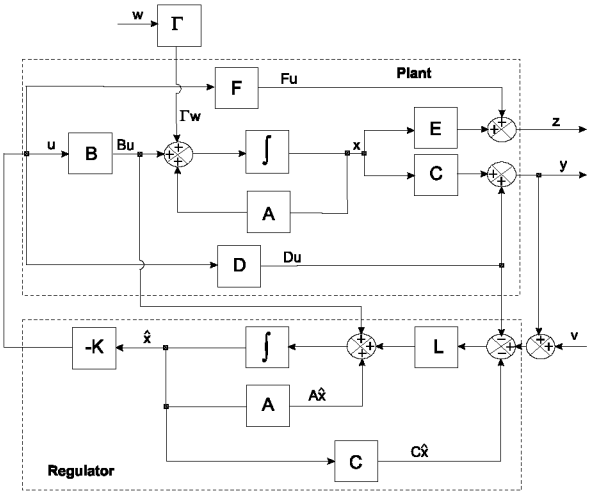

Figure 5: Block Diagram: Linear Quadratic Gaussian Regulator.

The preferred representation of the system for control design purpose was state-space, where the first and the second lines of Equation 1 were appended to the regulator dynamics,

$$\dot{\hat{x}} = A\hat{x} + Bu + L\left(y_v - C\hat{x} - Du\right) \qquad (4)$$
$$u = -K\hat{x}$$

yielding the following closed-loop equations,

$$\begin{Bmatrix} \dot{x} \\ \dot{\hat{x}} \end{Bmatrix} = \begin{bmatrix} A & -BK \\ LC & A - BK - LC \end{bmatrix} \begin{Bmatrix} x \\ \hat{x} \end{Bmatrix} + \begin{Bmatrix} \Gamma \\ 0 \end{Bmatrix} w \qquad (5)$$
$$\begin{Bmatrix} y \\ z \end{Bmatrix} = \begin{bmatrix} C & -DK \\ E & -FK \end{bmatrix} \begin{Bmatrix} x \\ \hat{x} \end{Bmatrix}$$

In the above equation, the single input variable is the buffet disturbance. Hence, the transfer function representation of the open-loop system obtained with NASTRAN needed to be converted into an equivalent state-space form. MATLAB routines based on methods described in Reference 9 were available to perform the task. In general, to avoid ill-conditioned matrices, MATLAB offered balancing transformations described in References 10 and 11.

The typical regulator was designed for performance in the bandwidth defined by 10 and 60 Hz, with roll-off at the lower and higher frequencies. The Separation Theorem of the classic LQE-LQR Optimal Control theory was used to obtain the Kalman filter and the full-state feedback gains. Emphasis in the control law synthesis was given to attenuate the dynamic response associated with both the first and second modes of the vertical fin (at 15 and 43 Hz).

Performance Calculations

The ultimate goal of the present investigation was to study control performance based on the ground vibration tests when the system transfer functions were directly measured. Therefore, in order to harmonize the present analyses, Equation 5 was not be used to evaluate the numerical results, but rather its transfer function equivalent.

For the open-loop case, Equation 2 gives:

$$z(s) = G_{22}(s)w(s) \tag{6}$$

Referring to Figure 3:

$$u(s) = H(s)y_v(s) \tag{7}$$

Substitution of Equation 7 into Equation 2 yields the closed-loop system transfer function:

$$G_c(s) = G_{21}(s)G_u(s) + G_{22}(s) \tag{8}$$

Hence,

$$z_c(s) = G_c(s)w(s) \tag{9}$$

In Equation 8, the transfer function relating the control signal to the disturbance is defined as:

$$G_u(s) = H(s)\left(I - G_{11}(s)H(s)\right)^{-1} G_{12}(s) \tag{10}$$

i. e.

$$u(s) = G_u(s)w(s) \tag{11}$$

The power spectral density (PSD) of the disturbance was a known input obtained from the flight tests. Due to hardware limitations, these PSD were band-limited. The frequency content lying outside of each one of the critical modes for buffeting was cut off (Figure 6). Furthermore, in the ground vibration tests, this PSD described the shaker input signal that excited the structure at a single point. Also, between the shaker and the structure there was a load cell (Figure 9). In this section, the PSD of the output of this load cell was assumed to correspond to the disturbance load applied to the NASTRAN model to simulate buffeting. The subsequent use of the product between Equations 6, 9 and 11 and their respective complex conjugates produced the PSD of the performance sensors in the open- and closed-loop cases, and the control signal, respectively:

$$PSD_{out} = \left|TransferFunction\right|^2 PSD_{in} \tag{12}$$

From these PSD, both the control effort RMS values of each actuator group (as a fraction of the maximum allowed by the hardware), and the ratio (closed- over open loop) of the RMS values of the performance sensors were obtained. These were the metrics used to access the performance. The other parameter to evaluate control system performance was the robustness to reject the disturbance under those different flight conditions.

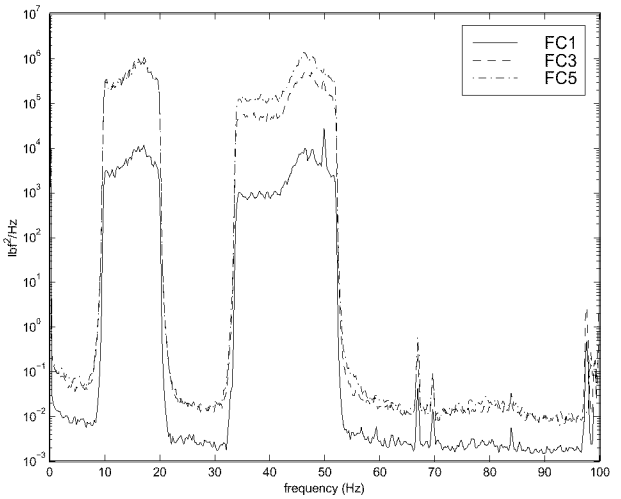

Figure 6: Power-Spectral-Density Functions for the Disturbance Input to the Shaker (Buffet Simulation for Flight Conditions FC1, FC3 and FC5).

Numerical Results

Control laws were synthesized based on NASTRAN numerical results using the method described in the previous sections. As a demonstration, a control law was designed using the feedback of the accelerometer A2 (situated at the trailing edge near the tip of the vertical fin) and strain gauge SG3 (located at the fin root near the rudder leading edge) – the critical location regarding fatigue effects. The results are summarized in Tables 3 to 5 for the buffet conditions listed in Table 2. The control law was synthesized based on data from FC1. Using the notation in Equation 1:

$$\begin{aligned} u &= \begin{bmatrix} G1 & G2 \end{bmatrix}^T \\ y &= \begin{bmatrix} A2 & SG3 \end{bmatrix}^T \\ z &= \begin{bmatrix} A2 & SG3 \end{bmatrix}^T \end{aligned} \tag{13}$$

Table 3: Control Law using Feedback of Accelerometer A2 and Strain Gauge SG3. Synthesis and Performance based on NASTRAN for FC1.

	Closed-/Open-loop RMS Values (%)		
	Mode 1	Mode 2	Modes 1 and 2
A2	68.5	48.3	65.2
SG3	67.4	30.3	40.3
	Control Effort 0-120 Hz (%)		
G1		90.2	
G2		100.0	

Table 4: Control Law using Feedback of Accelerometer A2 and Strain Gauge SG3. Synthesis and Performance based on NASTRAN for FC3.

	Closed-/Open-loop RMS Values (%)		
	Mode 1	Mode 2	Modes 1 and 2
A2	89.3	70.7	85.0
SG3	80.1	68.1	74.4
	Control Effort 0-120 Hz (%)		
G1		87.3	
G2		100.0	

Table 5: Control Law using Feedback of Accelerometer A2 and Strain Gauge SG3. Synthesis and Performance based on NASTRAN for FC5.

	Closed-/Open-loop RMS Values (%)		
	Mode 1	Mode 2	Modes 1 and 2
A2	93.2	81.1	89.9
SG3	89.7	82.7	87.6
	Control Effort 0-120 Hz (%)		
G1		89.2	
G2		100.0	

Experimental Setup

The IFOST rig in Australia was used for the ground vibration tests of the full-scale aircraft (Figure 7). The piezoelectric actuation devices were attached to both sides of the starboard vertical fin (Figure 8). A block diagram of the test setup is shown in Figure 9, from which one can observe the two banks of amplifies at each side of the fin driving the two groups of actuators acting in opposite phase to generate bending. The amplifiers fed the maximum voltage differential allowed across the piezoelectric devices (approximately 1500 V peak-to-peak). The third input signal was given by the 5000 lbf electromagnetic shaker attached to a single point at center of the starboard side of the fin through a load cell. Representative buffet time sequences associated with the different flight conditions analyzed were fed into the computer that controlled the shaker. A load cell was placed between the shaker and the structure to monitor the actual dynamic loads transmitted into the structure by the exciting mechanism.

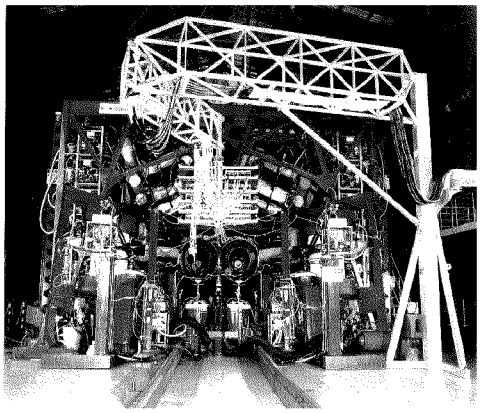

Figure 7: Full-Scaled Aircraft in the Australian IFOST Rig.

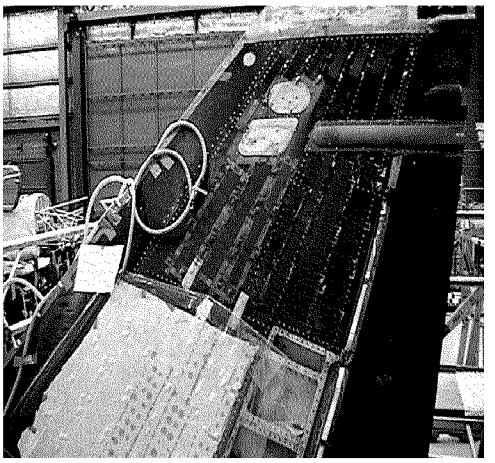

Figure 8: Instrumented Vertical Fin.

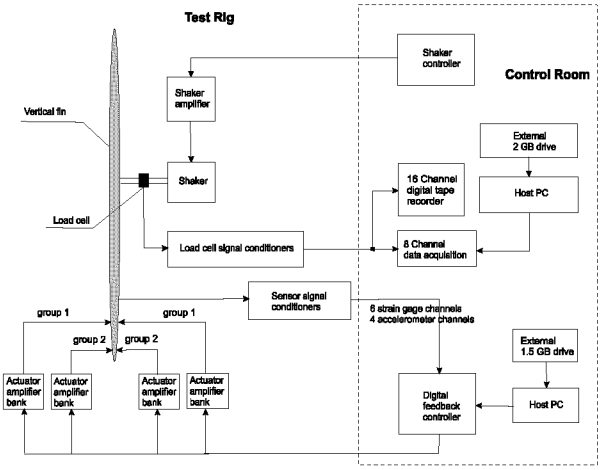

Figure 9: Block Diagram for the Test Set-Up.

Air bags partially inflated were used to simulate the aerodynamic damping provided by the motion-dependent airloads. Four accelerometers and six strain gauge rosettes situated at strategic points of the fin provided the output signals. In the control room, an 8-channel data acquisition system was used to acquire real-time frequency-domain data including transfer functions and auto-spectra. In addition, a 16-channel digital tape recorder was used to record data from all available signals for subsequent off-line analyses. The signal from two channels could be selected for feedback control through a computer driven DSP board.

System Identification

During the open-loop tests in September 1997, the standard technique of measuring system transfer functions by energizing each drive system (shaker and actuator groups) independently and measuring the sensor response provided unexpected results. These were ascribed to the internal damping of the large electrodynamic shaker changing the stiffness of the fin when not energized (a node was artificially forced at the shaker attachment point). Unfortunately, the magnitude of this damping was large compared to the singular effect of each actuator string thereby effectively masking the true transfer function. A solution to this problem was found by feeding all three input variables (actuator groups G1 and G2 and the buffet disturbance) using three simultaneous and independent random processes. However, this procedure slowed down the convergence of the transfer functions due to the increasing importance of the cross talk amongst drivers and transducers. Due to the fact that the shaker controller could only run relatively short time sequences, an unsatisfactory number of ensembles could be taken to determine the individual transfer functions. Therefore, optimization techniques were then required, obtaining the "best" estimate of the required transfer functions in a least square sense in terms of the cross- and power-spectral-densities measured between a given input and the correspondent output. In this case, the identification was performed in a 3×3 MIMO system where the third transducer was the load cell.

Experimental Results

Three control laws (CL1, CL2 and CL3) were designed based on open-loop test data using the feedback from different pairs of sensors. The identification of the sensors used and their respective participation in a determined control law is summarized in Table 6.

Table 6: Feedback Control Synthesis

sensor identification	approximate sensor position	control law identification
A1	fin tip, near leading edge	CL1
A2	fin tip, near trailing edge	CL1 & CL2
A3	1/3-span, near leading edge	none
A4	1/3-span, near rudder leading edge	none
SG3	fin root, near rudder leading edge (critical point)	CL2 & CL3
SG5	2/3-span, near rudder leading edge	CL3

Note: "A" defines accelerometer and "SG" strain gauge.

All control laws were designed based on open-loop test data for FC1. Tables 7 to 12 depict the control performance in the frequency intervals shown for control laws CL2 and CL3 that presented the best performance (the gain for control law CL1 was reduced during the tests due to indications of stability problems). The given intervals include modes 1, 2, and 1 and 2 together, respectively. The control effort as a fraction of the maximum allowed per group was calculated in the interval between 5 and 1000 Hz. In the same tables, both the estimated performance metric (using Equation 11) and the actually measured performance metric obtained in the closed-loop tests are listed. One can observe that the estimations in general show good agreement with the measured data. From this analysis, one can also observe that, in fact, actuator groups G1 and G2 had more authority over modes 1 and 2, respectively. The reduction in the vibration levels associated with mode 1 was in general less significant than those for mode 2, following the trend of lower control effort observed for group G1.

Table 7: CL2 (Feedback of Accelerometers A2 and Stain Gauge SG3). Performance based on Experimental Results for FC1.

	Closed-/Open-loop RMS Values (%)					
	5-25 Hz		25-100 Hz		5-100 Hz	
	Est.	Test	Est.	Test	Est.	Test
A1	72.4	68.3	71.2	72.7	71.5	71.8
A2	68.5	70.3	48.3	57.8	65.2	58.5
A3	73.4	68.3	57.7	59.8	58.2	60.1
A4	73.7	68.8	27.0	39.9	55.2	59.8
SG3	75.9	67.4	30.3	42.5	40.3	66.7
	Control Effort 5-1000 Hz (%)					
	Estimated			Test		
G1	90.2			81.3		
G2	100.0			97.1		

Table 8: CL2 (Feedback of Accelerometers A2 and Stain Gauge SG3). Performance based on Experimental Results for FC3.

	Closed-/Open-loop RMS Values (%)					
	5-25 Hz		25-100 Hz		5-100 Hz	
	Est.	Test	Est.	Test	Est.	Test
A1	91.0	92.5	92.7	94.2	92.0	95.5
A2	90.3	92.3	86.7	86.9	87.0	87.3
A3	92.2	92.2	83.3	88.1	85.9	88.4
A4	92.1	92.4	69.1	71.0	88.7	89.1
SG3	80.1	92.3	68.1	86.9	74.4	87.3
	Control Effort 5-1000 Hz (%)					
	Estimated			Test		
G1	83.7			81.4		
G2	100.0			107.5		

Table 9: CL2 (Feedback of Accelerometers A2 and Stain Gauge SG3). Performance based on Experimental Results for FC5.

	Closed-/Open-loop RMS Values (%)					
	5-25 Hz		25-100 Hz		5-100 Hz	
	Est.	Test	Est.	Test	Est.	Test
A1	92.4	94.4	92.0	92.3	92.3	92.6
A2	93.2	94.3	81.1	87.8	89.9	88.0
A3	92.9	93.9	86.3	88.7	87.9	88.8
A4	90.0	94.0	69.1	76.6	78.7	88.9
SG3	89.7	94.3	82.9	87.8	87.6	88.0
	Control Effort 5-1000 Hz (%)					
	Estimated			Test		
G1	89.2			99.3		
G2	100.0			97.1		

Table 10: CL3 (Feedback of Strain Gauges SG3 and SG6). Performance based on Experimental Results for FC1.

	Closed-/Open-loop RMS Values (%)					
	5-25 Hz		25-100 Hz		5-100 Hz	
	Est.	Test	Est.	Test	Est.	Test
A1	68.2	65.6	93.1	96.4	87.4	90.3
A2	68.2	64.8	86.2	84.9	85.5	84.9
A3	74.4	68.7	85.1	85.0	84.8	85.0
A4	70.5	67.3	69.1	66.7	69.8	66.7
SG3	74.5	70.0	72.8	67.2	74.2	69.6
	Control Effort 5-1000 Hz (%)					
	Estimated			Test		
G1	68.8			65.4		
G2	102.1			103.2		

Table 11: CL3 (Feedback of Strain Gauges SG3 and SG6). Performance based on Experimental Results for FC3.

	Closed-/Open-loop RMS Values (%)					
	5-25 Hz		25-100 Hz		5-100 Hz	
	Est.	Test	Est.	Test	Est.	Test
A1	92.5	92.5	99.8	98.6	97.2	96.6
A2	95.9	92.4	95.6	94.1	95.6	93.9
A3	94.7	93.2	94.1	94.3	94.1	94.3
A4	96.1	92.6	80.4	81.3	92.5	90.8
SG3	95.0	93.0	86.5	87.6	94.5	92.8
	Control Effort 5-1000 Hz (%)					
	Estimated			Test		
G1	61.4			53.4		
G2	102.4			98.1		

Table 12: CL3 (Feedback of Strain Gauges SG3 and SG6). Performance based on Experimental Results for FC5.

	Closed-/Open-loop RMS Values (%)					
	5-25 Hz		25-100 Hz		5-100 Hz	
	Est.	Test	Est.	Test	Est.	Test
A1	92.7	93.1	98.2	101.6	97.2	100.3
A2	92.5	93.0	95.1	98.2	95.0	98.0
A3	90.1	93.6	96.1	98.2	95.9	98.0
A4	94.7	93.1	79.6	84.4	88.9	90.5
SG3	96.2	92.6	88.5	92.4	95.4	92.6
	Control Effort 5-1000 Hz (%)					
	Estimated			Test		
G1	95.1			80.7		
G2	104.1			97.7		

Conclusions

An important step in the development of adaptive or "smart structures" system was given since for the first time a full-scale aircraft was tested aiming at buffet control using this new technology. Very promising results were obtained in the experimental work with a two-input, two-output controller using a standard linear time invariant LQG design. These results were based on a relatively simple method using NASTRAN to generate the aeroelastic transfer functions necessary for control law synthesis.

Vertical fin buffet attenuation approximately 60% for the nominal flight configuration FC1 and 30% for the most severe case FC5 was observed during the tests. Also, very significant vibration reduction measured by the most important performance metric – the strain gauge located at the critical point for fatigue (SG3) was verified for FC5: 17.1% (Mode 2) and 12.0% (Modes 1 and 2). In general, the control laws that included at least one strain gauge in the feedback loop revealed better performance. In fact, CL2 comprising feedback from one accelerometer situated at the tip of the fin and SG3 presented the best results. This is an indication that strain gauges can be better co-related to the control objective, which is to reduce the structural strain generated by buffeting. The method showed that the general trends of the system can be reproduced numerically, and it may be useful in preliminary analyses.

References

1. Zimmerman, N. H., Ferman, M. A., Yurkovich, R. N. and Gerstenkorn, G., "Prediction of Tail Buffet Loads for Design Application," *AIAA/ASME/ASCE/ AHS/ASC 30th Structures, Structural Dynamics and Materials Conference*, American Institute of Aeronautics and Astronautics, Washington, DC, pp. 1911-1919.
2. Ferman, M. A., Patel, S. R., Zimmerman, N. H. and Gerstenkorn, G., "A Unified Approach to Buffet Response of Fighter Aircraft Empennage," *Aircraft Dynamic Loads due to Flow Separation*, AGARD Report CP-483, North Atlantic Treaty Organization, Neuilly-Sur-Seine, France, September 1990, pp. 2.1-2.18.
3. Lee, B. H. K., Brown, D., Zgela, M. and Poirel, D., "Wind Tunnel and Flight Tests of Tail Buffet on the CF-18 Aircraft," *Aircraft Dynamic Loads due to Flow Separation,* AGARD Report CP-483, North Atlantic Treaty Organization, Neuilly-Sur-Seine, France, September 1990, pp. 1.1-1.26.
4. Edwards, J. W., "Unsteady Airloads Due to Separated Flow on Airfoils and Wings," *Aircraft Dynamic Loads due to Flow Separation*, AGARD Report CP-483, North Atlantic Treaty Organization, Neuilly-Sur-Seine, France, September 1990, pp. 16.1-16.18.
5. Albano, E., and Rodden, W. P., "A Doublet-Lattice Method for Calculating Lift Distributions on Oscillating Surfaces in Subsonic Flows," *AIAA Journal*, Vol. 7, pp. 279-285, 1969.
6. Rock, S. M., Ashley, H., Digumarthi, R. and Chaney, K., "Active Control for Fin Buffet Alleviation," in *Advances in Aerospace Sciences: A Tribute to Prof. Holt Ashley*, P. Hagela and S. C. McIntosh, Jr. Editors, Stanford University, 1993, pp. 413-421.
7. Nitzsche, F., Zimcik, D. G. and Langille, K. "Active Control of Vertical Fin Buffeting with Aerodynamic Control Surface and Strain Actuation," *AIAA/ASME/AHS Adaptive Structures Forum*, Kissimmee, FL, April 7-10, 1997, American Institute of Aeronautics and Astronautics, Washington DC, CP973, pp. 1467-1477.
8. Moses, R. W., "Vertical fin buffeting alleviation using piezoelectric actuators," in *Smart Structures and Materials 1997, Industrial and Commercial Applications of Smart Structures Technologies*, J. M. Sater, Ed., SPIE Vol. 3044.
9. Kailath, T., *Linear Systems*, Prentice-Hall, NJ, 1980, pp. 345-370.
10. Laub, A. J. *et al.* "Computation of System Balancing Transformations and Other Applications of Simultaneous Diagonalization Algorithms," *IEEE Transactions on Automatic Control*, AC-32, 1987, pp. 115-122.
11. Moore, J. B., "Principal Component Analysis in Linear Systems: Controllability, Observability and Model Reduction, "*IEEE Transactions on Automatic Control*, AC-26, 1981, pp. 17-31.